Minimization of entropy generation due to MHD double diffusive mixed convection in a lid driven trapezoidal cavity with various aspect ratios

Priyajit Mondal, Tapas Ray Mahapatra[1,2]

Department of Mathematics, Visva-Bharati (A Central University),
Santiniketan – 731 235, West-Bengal, India
priyajit.math@gmail.com; trmahapatra@yahoo.com

Abstract. Entropy generation minimization has significant importance in fluid flow, heat and mass transfer in an enclosure to get the maximum efficiency of a system and to reduce the loss of energy. In the present study, the analysis of mixed convection fluid flow, heat and mass transfer with heat line and mass line concept and entropy generation due to the effects of fluid flow, heat flow, mass flow and magnetic field in a trapezoidal enclosure with linearly heated and diffusive left wall, uniformly heated and diffusive lower wall, cold and nondiffusive right wall, adiabatic and zero diffusion gradient top wall have been reported. Parametric studies for the wide range of Prandtl number ($Pr = 0.7$ for air cooling system and $Pr = 1000$ for the engines filled with olive or engine oils), Rayleigh number ($Ra = 10^3 - 10^5$), aspect ratio ($A = 0.5 - 1.5$) and inclination angle of the cavity ($\phi = 45\,°-90\,°$) have been performed, which help to construct the perfect shape of cavity in many engineering and physical applications so that the entropy is minimum to get the maximum efficiency of any system. The finite-difference approximation has been used to find out the numerical solutions. Biconjugate Gradient Stabilized (BiCGStab) method is used to solve the discretized nonhomogeneous system of linear equations.

Keywords: mixed convection flow, heat transfer, mass transfer, heat line, mass line, entropy generation, lid driven trapezoidal enclosure, magnetic field, aspect ratio.

1 Introduction

Mixed convection is a combination of forced convection and natural convection, which exists when a flow is determined simultaneously by both an outer forcing system and inner volumetric forces. In many engineering applications, engineers often encounter forced convection to design or analyze heat exchangers, pipe flow, cavity flow, flow over a flat plate etc. If the natural convection is not much less than the forced convection,

---

    [2]Corresponding author.

then the flow is considered as mixed convection flow. In any mixed convection, flow stream lines, heat lines and mass lines are routinely considered as very efficient method for the adequate visualization tools of fluid flow, heat transfer and mass transfer, respectively. The heat function and heat line concept were first introduced by Kimura and Bejan [19] to visualize the heat transfer phenomena and in the field of mass transfer, mass function and mass line concept were first discussed by Trevisan and Bejan [35]. Heat and mass transfer phenomena have received considerable attention due to its various engineering and natural applications such as air cooling [10, 14], heat exchanger [33], solar plate collector [36], geothermal system [7] etc. Air cooling is mostly preferable method for the cooling of computer system and other electronic equipments because of its simplicity and low cost. Lid-driven cavity flow is also very important due to its applications in crystal growth, flow and heat transfer in solar ponds [9], dynamics of lakes [18], thermal hydraulics of nuclear reactors [16], food processing and float glass production [25] etc. One useful control parameter for convective heat and mass transfer in cavities is magnetic field. Effect of magnetic field on double diffusive natural convection heat transfer in trapezoidal enclosure has been discussed by Teamah and Shehata [34]. Sensitivity analysis on MHD heat transfer and entropy generation in inclined trapezoidal cavity filled with nanofluid has been discussed by Shirvan et al. [2]. Together with these analyses, it is also very important to save energy. The second law of thermodynamics analyzes and estimates the efficiency of a thermal system, which states that when energy is transformed from one state to another, there is a loss in the amount of available energy, which reduces the efficiency of the system. In order to minimize the irreversibilities associated with the system, a new methodology is improved, known as entropy generation minimization. Therefore, it is important to analyze the entropy generation minimization to increase the efficiency of the system. Many researches have been done on this topic. Entropy generation minimization concept was first introduced by Bejan [4–6]. The heat transfer rate and entropy generation due to heat transfer and fluid friction during natural convection in trapezoidal enclosures have been discussed by Basak et al. [3]. Ramakrishna et al. [26] analysed the entropy generation during free convection within trapezoidal cavity. Singh et al. [32] investigated the role of entropy generation on thermal management during natural convection in tilted porous square cavities. A numerical analysis of double-diffusive MHD natural convection and entropy generation inside a tilted sinusoidal corrugated porous enclosure has been discussed by Hussain [15].

Recently, entropy generation in natural convection of nanofluid inside a square cavity having hot solid block has been analyzed by Sheremet et al. [30]. Sheremet et al. [31] also discussed natural convection of nanofluid inside a wavy cavity with a nonuniform heating. More recently, using Buongiorno's mathematical model, Sheremet et al. [29] discussed natural convection and entropy generation in a square cavity with side walls having variable temperature filled with a nanofluid. The natural convection flow with hot horizontal wall and an adjacent cold vertical wall has an important application in the heat transfer analysis of electronic equipment, mainly in slim rack described by Carvalho et al. [8]. In this case, the power dissipation from the horizontal circuit board is limited by its temperature. MHD mixed convection in a flexible walled and nanofluids filled lid-driven cavity with volumetric heat generation has been analyzed by Selimefendigil and Öztop

[28]. Hasanuzzaman et al. [13] discussed magnetohydrodynamic natural convection in trapezoidal cavities. Effects of moving lid direction on MHD mixed convection in a linearly heated cavity have been studied by Al-Salem et al. [1]. Raza et al. [27] examined the combined effects of thermal radiation and magnetic field on molybdenum disulfide nanofluid in a channel with changing walls. A numerical model of MHD stability of natural convection in a cylindrical configuration filled with fluid is studied by Oudina and Bessaïh [23]. Numerical simulation of the effect of Prandtl number on oscillatory MHD natural convection in cylindrical annulus is discussed by Oudina and Makinde [24]. Oudina [22] modeled numerically the hydrodynamic stability in vertical annulus having heat source of different lengths. Recently, Alkasassbeh et al. [2] studied the heat transfer of convective fin with temperature dependent internal heat generation by hybrid block method.

In the present study, mixed convection fluid flow, heat and mass transfer with heat line and mass line concept and entropy generation minimization have been analyzed. The main objective of the present study is the analysis of entropy generation due to heat transfer, mass transfer and magnetic field and the total entropy generation in a trapezoidal enclosure with various aspect ratios in which the upper wall of the cavity is moving with a constant velocity. Our purpose is to analyze the thermal behavior of the fluid inside the trapezoidal enclosure under the effect of various parameters in terms of stream line, isotherm, isoconcentration, heat line, mass line, entropy generation due to heat transfer, fluid friction, mass transfer and magnetic field. The goal of our study is to achieve minimum entropy generation in order to enhance the overall efficiency of the system.

2 Problem formulation

A trapezoidal cavity filled with incompressible viscous fluid, with right and left walls inclined at an angle ϕ with the positive x-axis and negative x-axis, respectively, has been considered with uniformly heated and massive bottom wall, adiabatic and of zero concentration gradient top wall, hot and diffusive side walls. The nondimensional governing equations for two-dimensional, double-diffusive, steady, mixed convection flow in the presence of magnetic field can be written from the dimensional governing equations in [15] with the help of following nondimensional quantities: $x = X/L$, $y = Y/L$, $u = UL/\alpha$, $v = VL/\alpha$, $\theta = (T - T_c)/(T_h - T_c)$, $p = PL^2/(\rho\alpha^2)$, $Pr = \nu/\alpha$, $Le = \alpha/D$, $Ra = g\beta_T(T_h - T_c)L^3/\nu\alpha$, $S = (C - C_c)/(C_h - C_c)$, $Ha = BL\sqrt{(\sigma/\mu)}$, $N = (\beta_S(C_h - C_c))/(\beta_T(T_h - T_c))$ as follows. Equation of continuity:

$$\frac{\partial u}{\partial x} + \frac{\partial v}{\partial y} = 0,$$

momentum equations:

$$u\frac{\partial u}{\partial x} + v\frac{\partial u}{\partial y} = -\frac{\partial p}{\partial x} + Pr\left[\frac{\partial^2 u}{\partial x^2} + \frac{\partial^2 u}{\partial y^2}\right] - Ha^2 Pr\, u, \tag{1}$$

$$u\frac{\partial v}{\partial x} + v\frac{\partial v}{\partial y} = -\frac{\partial p}{\partial y} + Pr\left[\frac{\partial^2 v}{\partial x^2} + \frac{\partial^2 v}{\partial y^2}\right] + RaPr(\theta + NS), \tag{2}$$

where X, Y are dimensional distances along the coordinate axes; U, V, T and C are dimensional velocities along x and y directions, temperature and concentration, respectively; x and y are dimensionless distances along x and y coordinates, respectively; u, v, θ and S are dimensionless velocities along x and y coordinates, temperature and concentration, respectively; L is the length of the enclosure, α is the thermal diffusivity, β_T is the coefficient of thermal expansion, β_S is the coefficient of solutal expansion, T_h and T_c are the temperature at the hot and cold wall, respectively; C_c and C_h are low and high concentrations at the wall of the cavity, respectively; ν is the kinematic viscosity, P is the dimensional pressure, p is the dimensionless pressure, ρ is the fluid density, g is the acceleration due to gravity, B is the magnetic induction, Pr is the Prandtl number, Ra is the Rayleigh number, Ha is the Hartmann number, N is buoyancy ratio, D is mass diffusivity, σ is electrical conductivity. The upper wall of the cavity is moving with a constant velocity $U_0 = \alpha/L$ towards positive x direction.

Using stream function (ψ) and vorticity function (ω), momentum Eqs. (1) and (2) yield governing equation of vorticity

$$u\frac{\partial \omega}{\partial x} + v\frac{\partial \omega}{\partial y} = Pr\left[\frac{\partial^2 \omega}{\partial x^2} + \frac{\partial^2 \omega}{\partial y^2}\right] + RaPr\left[\frac{\partial \theta}{\partial x} + N\frac{\partial S}{\partial x}\right] + Ha^2 Pr\frac{\partial u}{\partial y} \qquad (3)$$

and governing equation of stream function

$$\frac{\partial^2 \psi}{\partial x^2} + \frac{\partial^2 \psi}{\partial y^2} = -\omega. \qquad (4)$$

Eliminating ω from (3) and (4), we get biharmonic equation of ψ as

$$Pr\left[\frac{\partial^4 \psi}{\partial x^4} + 2\frac{\partial^4 \psi}{\partial x^2 \partial y^2} + \frac{\partial^4 \psi}{\partial y^4}\right] + \frac{\partial \psi}{\partial y}\left[\frac{\partial^3 \psi}{\partial x^3} + \frac{\partial^3 \psi}{\partial x \partial y^2}\right] - \frac{\partial \psi}{\partial x}\left[\frac{\partial^2 \psi}{\partial x^2 \partial y} + \frac{\partial^3 \psi}{\partial y^3}\right]$$
$$- RaPr\left[\frac{\partial \theta}{\partial x} + N\frac{\partial S}{\partial x}\right] - Ha^2 Pr\frac{\partial^2 \psi}{\partial y^2} = 0. \qquad (5)$$

Temperature equation:
$$u\frac{\partial \theta}{\partial x} + v\frac{\partial \theta}{\partial y} = \left[\frac{\partial^2 \theta}{\partial x^2} + \frac{\partial^2 \theta}{\partial y^2}\right]. \qquad (6)$$

Concentration equation:
$$u\frac{\partial S}{\partial x} + v\frac{\partial S}{\partial y} = \frac{1}{Le}\left[\frac{\partial^2 S}{\partial x^2} + \frac{\partial^2 S}{\partial y^2}\right]. \qquad (7)$$

Equations of heat function:
$$\frac{\partial \pi}{\partial y} = u\theta - \frac{\partial \theta}{\partial x}, \quad -\frac{\partial \pi}{\partial x} = v\theta - \frac{\partial \theta}{\partial y},$$

which yield a single equation

$$\frac{\partial^2 \pi}{\partial x^2} + \frac{\partial^2 \pi}{\partial y^2} = \frac{\partial}{\partial y}(u\theta) - \frac{\partial}{\partial x}(v\theta). \qquad (8)$$

Equations of mass function:

$$\frac{\partial \tau}{\partial y} = uS - \frac{\partial S}{\partial x}, \quad -\frac{\partial \tau}{\partial x} = vS - \frac{\partial S}{\partial y},$$

which yield a single equation

$$\frac{\partial^2 \tau}{\partial x^2} + \frac{\partial^2 \tau}{\partial y^2} = \frac{\partial}{\partial y}(uS) - \frac{\partial}{\partial x}(vS), \tag{9}$$

where Le is the Lewis number, π is the heat function and τ is the mass function. The boundary conditions are as follows:

(i) At the top wall: $u=1$ (lid-driven upper wall), $v=0$ (no slip condition), $\partial\theta/\partial y=0$ (adiabatic condition), $\partial S/\partial y = 0$ (zero concentration gradient), $\pi = 0$, $\tau = 0$.

(ii) At the bottom wall: $u = v = 0$ (no slip conditions), $\theta = 1$ (uniformly heated), $S = 1$ (uniformly diffusive), $\hat{n} \cdot \nabla\pi = 0$ (uniform heating), $\hat{n} \cdot \nabla\tau = 0$ (uniformly diffusive),

$$\pi = \begin{cases} \frac{\overline{Nu_l}}{\sin\phi} & \text{(left bottom corner)}, \\ -\frac{\overline{Nu_r}}{\sin\phi} & \text{(right bottom corner)}, \end{cases}$$

$$\tau = \begin{cases} \frac{\overline{Sh_l}}{\sin\phi} & \text{(left bottom corner)}, \\ -\frac{\overline{Sh_r}}{\sin\phi} & \text{(right bottom corner)}, \end{cases}$$

where $\overline{Nu_l}$ and $\overline{Nu_r}$, $\overline{Sh_l}$ and $\overline{Sh_r}$ are given in Sections 3 and 4.

(iii) At the left wall: $u = v = 0$ (no slip conditions), $\theta = 1 - y$ (linearly heated), $S = 1 - y$ (linearly diffusive), $\hat{n} \cdot \nabla\pi = \sin\phi$, $\hat{n} \cdot \nabla\tau = \sin\phi$.

(iv) At the right wall: $u = v = 0$ (no slip conditions), $\theta = 0$ (cold), $S = 0$ (nondiffusive), $\hat{n} \cdot \nabla\pi = 0$, $\hat{n} \cdot \nabla\tau = 0$, where $\hat{n}$ denotes the unit normal vector to the wall.

3   Heat transfer

Nusselt number (Nu) is the ratio of heat transferred due to convection and the heat transferred due to conduction, and so it tells us about how much the heat transfer is enhanced due to fluid motion. It is a nondimensional heat transfer coefficient, which is mathematically defined as $Nu = -\partial\theta/\partial n$, where n denotes normal direction to a plane. The local Nusselt number at the top, bottom, left and right walls of the cavity are, respectively, defined by

$$Nu_t = -\frac{\partial\theta}{\partial y}\bigg|_{y=A}, \qquad Nu_b = \frac{\partial\theta}{\partial y}\bigg|_{y=0},$$

$$Nu_l = \frac{\partial\theta}{\partial x}\bigg|_l \sin\phi + \frac{\partial\theta}{\partial y}\bigg|_l \cos\phi, \qquad Nu_r = -\frac{\partial\theta}{\partial x}\bigg|_r \sin\phi + \frac{\partial\theta}{\partial y}\bigg|_r \cos\phi$$

and the average Nusselt number at bottom, left, right walls and average Nusselt number are given by

$$\overline{Nu_b} = \int\limits_0^1 Nu_b \, \mathrm{d}x, \qquad \overline{Nu_l} = \frac{\sin\phi}{A} \int\limits_0^{A/\sin\phi} Nu_l \, \mathrm{d}S_1,$$

$$\overline{Nu_r} = \frac{\sin\phi}{A} \int\limits_0^{A/\sin\phi} Nu_r \, \mathrm{d}S_2 \quad \text{and} \quad \overline{Nu} = \frac{\overline{Nu_b} + \overline{Nu_l} + \overline{Nu_r}}{3},$$

respectively, where $\mathrm{d}S_1$ and $\mathrm{d}S_2$ are the small elemental lengths along the left and right walls, respectively. Here, since top wall is considered to be adiabatic, so $Nu_t = 0$.

4 Mass transfer

Sherwood Number (Sh) is the ratio of the convective mass transfer and the diffusive mass transport, and so it tells us about how much mass transfer is enhanced due to fluid motion. It is a nondimensional mass transfer coefficient, which is mathematically defined as $Sh = -\partial S/\partial n$, where n and S denote normal direction to a plane and nondimensional concentration, respectively. The local Sherwood number at the top, bottom, left and right walls of the cavity are, respectively, given by

$$Sh_t = -\frac{\partial S}{\partial y}\bigg|_{y=A}, \qquad Sh_b = \frac{\partial S}{\partial y}\bigg|_{y=0},$$

$$Sh_l = \sin\phi \frac{\partial S}{\partial x}\bigg|_l + \cos\phi \frac{\partial S}{\partial y}\bigg|_l, \qquad Sh_r = -\sin\phi \frac{\partial S}{\partial x}\bigg|_r + \cos\phi \frac{\partial S}{\partial y}\bigg|_r,$$

and the average Sherwood number at bottom, left, right walls and average Sherwood numbers at the corresponding walls of the cavity are given by

$$\overline{Sh_b} = \int\limits_0^1 Sh_b \, \mathrm{d}x, \qquad \overline{Sh_l} = \frac{\sin\phi}{A} \int\limits_0^{A/\sin\phi} Sh_l \, \mathrm{d}S_1,$$

$$\overline{Sh_r} = \frac{\sin\phi}{A} \int\limits_0^{A/\sin\phi} Sh_r \, \mathrm{d}S_2 \quad \text{and} \quad \overline{Sh} = \frac{\overline{Sh_b} + \overline{Sh_l} + \overline{Sh_r}}{3},$$

respectively, where $\mathrm{d}S_1$ and $\mathrm{d}S_2$ are the small elemental lengths along the left and right walls, respectively. Here, since top wall is considered to be of zero diffusive gradient, so $Sh_t = 0$.

5 Entropy generation

Entropy, generated by fluid friction, heat transfer and mass transfer are discussed by Mourad et al. [21], and the effect of magnetic field on entropy generation has been

discussed by Hussain [4]. The dimensionless forms of local entropy generations due to fluid friction (S_ψ), thermal gradients (S_θ), diffusion (S_τ) and magnetic field (S_M) are, respectively, given by

$$S_\psi = \lambda_1 \left[2\left(\left(\frac{\partial u}{\partial x}\right)^2 + \left(\frac{\partial v}{\partial y}\right)^2 \right) + \left(\frac{\partial u}{\partial y} + \frac{\partial v}{\partial x}\right)^2 \right], \tag{10}$$

$$S_\theta = \left(\frac{\partial \theta}{\partial x}\right)^2 + \left(\frac{\partial \theta}{\partial y}\right)^2, \tag{11}$$

$$S_\tau = \lambda_2 \left[\left(\frac{\partial S}{\partial x}\right)^2 + \left(\frac{\partial S}{\partial y}\right)^2 \right] + \lambda_3 \left[\frac{\partial \theta}{\partial x}\frac{\partial S}{\partial x} + \frac{\partial \theta}{\partial y}\frac{\partial S}{\partial y} \right], \tag{12}$$

$$S_M = \lambda_1 Ha^2 u^2, \tag{13}$$

where λ_1, λ_2 and λ_3 are called irreversibility distribution ratios. In the present study, the values of λ_1, λ_2 and λ_3 are taken as 10^{-4}, 0.5 and 0.01, respectively.

6 Coordinate transformation and numerical procedure

Application of boundary conditions at various boundaries of an enclosure with complex geometry is a difficult tusk. In order to reduce the complexity of such situation, we use transformations to get a simple computational region. In the present study, the physical domain (trapezoidal domain in x, y-plane) has been transformed into the computational domain (square in ξ, η-plane) by using the following transformations (see Fig. 1):

$$\xi = \frac{x + y \cot\phi}{1 + 2y \cot\phi}, \quad y = A\eta, \tag{14}$$

where A is the aspect ratio, ξ and η are horizontal and vertical coordinates in a unit square. Now it becomes very easier to obtain the finite-difference representation of the governing equations in the computational domain to solve the equations. Using the transformation (14), Eqs. (5)–(9) are transformed as:

$$PrF^2\psi_{\xi\xi\xi\xi} + 2PrEF\psi_{\xi\xi\xi\eta} + T_5\psi_{\xi\xi\eta\eta} + 2\frac{PrE}{A^2}\psi_{\xi\eta\eta\eta} + \frac{Pr}{A^4}\psi_{\eta\eta\eta\eta}$$
$$+ T_1\psi_{\xi\xi\xi} + T_2\psi_{\xi\xi\eta} + T_3\psi_{\xi\eta\eta} - \frac{v}{A^3}\psi_{\eta\eta\eta} + T_4\psi_{\xi\xi} + T_6\psi_{\xi\eta} + T_7\psi_\xi$$
$$- RaPrG\theta_\xi - RaPrGNS_\xi - Ha^2Pr\left[\frac{AE}{2}u_\xi + \frac{1}{A}u_\eta\right] = 0, \tag{15}$$

$$F\theta_{\xi\xi} + E\theta_{\xi\eta} + \frac{1}{A^2}\theta_{\eta\eta} - B_K\theta_\xi - \frac{v}{A}\theta_\eta = 0, \tag{16}$$

$$FS_{\xi\xi} + ES_{\xi\eta} + \frac{1}{A^2}S_{\eta\eta} - B_{Kc}S_\xi - \frac{v}{A}S_\eta Le = 0, \tag{17}$$

$$F\pi_{\xi\xi} + E\pi_{\xi\eta} + \frac{1}{A^2}\pi_{\eta\eta} + H\pi_\xi$$
$$= \left(\frac{EA}{2}u - vG\right)\theta_\xi + \frac{u}{A}\theta_\eta + \frac{EA}{2}\theta u_\xi + \frac{\theta}{A}u_\eta - G\theta v_\xi, \tag{18}$$
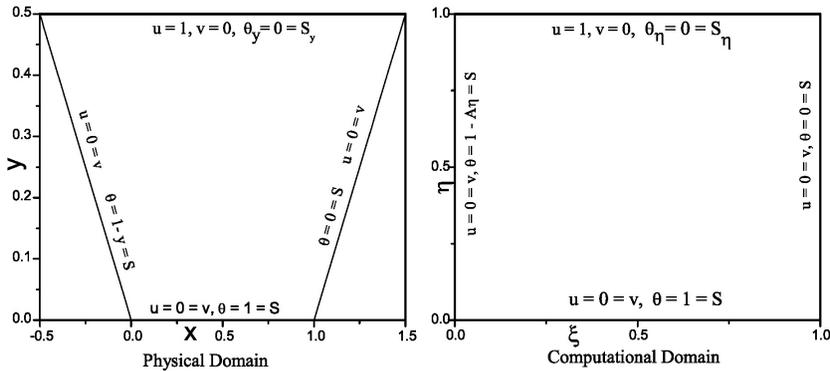
Figure 1. Schematic diagram of physical and computational domain for $A = 0.5$ and $\phi = 45\,^\circ$.

$$F\tau_{\xi\xi} + E\tau_{\xi\eta} + \frac{1}{A^2}\tau_{\eta\eta} + H\tau_\xi$$
$$= \left(\frac{EA}{2}u - vG\right)S_\xi + \frac{u}{A}S_\eta + \frac{EA}{2}Su_\xi + \frac{S}{A}u_\eta - GSv_\xi, \tag{19}$$

and the expressions of entropy generation due to fluid friction (10), heat transfer (11), mass transfer (12) and magnetic effect (13) can be expressed, respectively, in ξ, η-coordinate system as

$$S_\psi = \lambda_1\left[\left(2G^2 + \frac{A^2E^2}{4}\right)u_\xi^2 + \frac{1}{A^2}u_\eta^2\left(\frac{A^2E^2}{4} + G^2\right)v_\xi^2 + \frac{2}{A^2}v_\eta^2\right.$$
$$\left. + Eu_\xi u_\eta + 2Ev_\xi v_\eta\right] + \lambda_1\left[AEGu_\xi v_\xi + \frac{2G}{A}u_\eta v_\xi\right],$$

$$S_\theta = \left(G^2 + \frac{A^2E^2}{4}\right)\theta_\xi^2 + \frac{1}{A^2}\theta_\eta^2 + E\theta_\xi\theta_\eta,$$

$$S_\tau = \lambda_2\left[\left(G^2 + \frac{A^2E^2}{4}\right)S_\xi^2 + \frac{1}{A^2}S_\eta^2 + ES_\xi S_\eta\right]$$
$$+ \lambda_3\left[\left(G^2 + \frac{A^2E^2}{4}\right)\theta_\xi S_\xi + \frac{E}{2}\left(\theta_\xi S_\eta + \theta_\eta S_\xi\right) + \frac{1}{A^2}\theta_\eta S_\eta\right]$$

and

$$S_M = \lambda_1 Ha^2 u^2,$$

where expressions for $E, F, G, H, T_1, T_2, T_3, T_4, T_5, T_6, T_7, B_K$ and B_{KC} are given in Appendix. The total entropy generation is given by

$$S_T = S_\psi + S_\theta + S_\tau + S_M.$$

Since Eqs. (15)–(19) are highly nonlinear, no analytical method is available to solve them. So, Eqs. (15)–(19) are solved numerically using finite-difference approximation

method. Using second-order approximations of different derivatives of stream function, temperature, concentration, heat function and mass function (see [20]), the discretizations of Eqs. (15)–(19) can be written in matrix form as

$$M_1 \boldsymbol{\psi} = \boldsymbol{f_1}(Pr, Ra, Ha, N, A, u, v, \theta, \psi_\xi, \psi_\eta, S), \tag{20}$$

$$M_2 \boldsymbol{\theta} = \mathbf{0}, \qquad M_3 \boldsymbol{S} = \mathbf{0}, \tag{21}$$

$$M_4 \boldsymbol{\pi} = \boldsymbol{f_2}(u, v, \theta, A), \qquad M_5 \boldsymbol{\tau} = \boldsymbol{f_3}(u, v, S, A), \tag{22}$$

where M_1, M_2, M_3, M_4 and M_5 are the coefficient matrices of order mn, $\boldsymbol{\psi}$, $\boldsymbol{\theta}$, $\boldsymbol{S}$, $\boldsymbol{\pi}$, $\boldsymbol{\tau}$, $\boldsymbol{f_1}$, $\boldsymbol{f_2}$ and $\boldsymbol{f_3}$ are mn-component vectors for a grid size $m \times n$. Equations (20)–(22) are solved by outer–inner iteration technique, which was discussed by Gupta and Kalita [12]. In a typical outer cycle, we solve Eqs. (20)–(22) using biconjugate gradient stabilized method (BiCGStab) [11], which constitutes inner iterations. Once Eqs. (20)–(22) are solved, we solve the tridiagonal linear systems arising from fourth-order finite-difference approximations of $(\psi_\xi)_{ij}$, $(\psi_\eta)_{ij}$, $(\theta_\xi)_{ij}$, $(\theta_\eta)_{ij}$, $(S_\xi)_{ij}$, $(S_\eta)_{ij}$, $(\pi_\eta)_{ij}$, $(\pi_\xi)_{ij}$, $(\tau_\xi)_{ij}$ and $(\tau_\eta)_{ij}$ to get the values of $(\psi_\xi)_{ij}$, $(\psi_\eta)_{ij}$, $(\theta_\xi)_{ij}$, $(\theta_\eta)_{ij}$, $(S_\xi)_{ij}$, $(S_\eta)_{ij}$, $(\pi_\eta)_{ij}$, $(\pi_\xi)_{ij}$, $(\tau_\xi)_{ij}$ and $(\tau_\eta)_{ij}$ as discussed by Mahapatra et al. [20]. This constitutes one outer cycle. We utilize a relaxation parameter λ inside both the inner as well as outer cycles for ψ, θ, S, π and τ. Then $u_{i,j}$ and $v_{i,j}$ are obtained from the relation of stream function with velocity components. The process continues till the maximum values of ψ_{error}, θ_{error}, S_{error}, π_{error} and τ_{error} between two iterations are less than 0.5×10^{-6}. At last, the entropy generations (S_ψ), (S_θ), (S_τ) and (S_M) are obtained from the discretized forms of Eqs. (10)–(13).

7 Results and discussion

The detailed discussion of stream functions, isotherms, isoconcentrations, heat lines, mass lines and entropy generation minimization for mixed convection flow within a lid-driven trapezoidal enclosure are illustrated in the present study. Till now entropy generation due to fluid friction, heat transfer, mass transfer and magnetic field in a lid-driven trapezoidal enclosure with various aspect ratios have not been discussed in any earlier researches. In order to check the accuracy of present result, a comparison has been made with the bench mark numerical solutions given by Basak et al. [3] and Davis [11]. The comparison has been made by the values of $|\psi|_{\max}$ and $\overline{Nu}$ (Table 1) within a square cavity with hot left wall, cold right wall, adiabatic top and bottom walls with $Pr = 0.71$ and $Ra = 10^3, 10^4, 10^5$. The computation has been done using grid size 81×81 and gives an excellent agreement with the results of Basak et al. [3] and Davis [11]. Also two graphical comparisons of stream function (ψ) and isotherm (θ) contours with Basak et al. [3] (Fig. 2) and the entropy generation contours due to fluid friction (S_ψ) and heat transfer (S_θ) with Hussain [15] and Ilis et al. [17] (Fig. 3) have been carried out. The excellent agreement can be seen. To check the convergence of the solution grid independence tests of $|\psi|_{\max}$, $|\pi|_{\max}$ and $|\tau|_{\max}$ with different grid sizes have been performed (Table 2) in which almost same results have been found for different grid sizes.
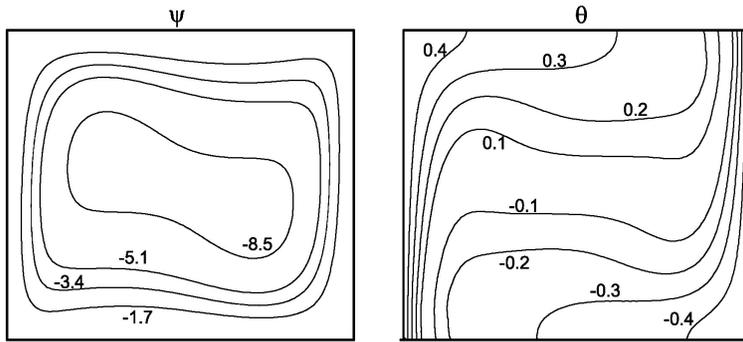
Figure 2. Stream function (ψ) and isotherm (θ) contours within a square cavity with hot left side wall, cold right sidewall, adiabatic top and bottom walls for $Ra = 10^5$ and $Pr = 0.7$.
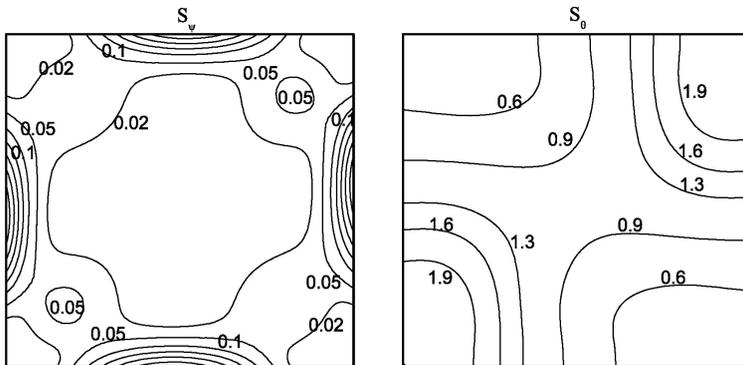
Figure 3. Entropy generation due to fluid friction (S_ψ) and heat transfer (S_θ) contours within a square cavity with hot left side wall, cold right side wall, adiabatic top and bottom walls for $Ra = 10^3$ and $Pr = 0.7$.

Table 1. Comparison of the present results with the results of Basak et al. [3] and Davis [11] for $Pr = 0.71$, $\phi = 0$, $Ha = 0$.

Ra	$|\psi|_{\max}$	$\overline{Nu}$	$|\psi|_{\max}$	$\overline{Nu}$	$|\psi|_{\max}$	$\overline{Nu}$
	Davis [11]		Basak et al. [3]		Present	
10^3	–	1.118	1.1746	1.1179	1.1727	1.1183
10^4	–	2.243	5.0737	2.2482	5.0745	2.2446
10^5	9.612	4.519	9.6158	4.5640	9.6217	4.5337

Stream lines, isotherms, isoconcentrations, heat lines, mass lines and entropy generation due to the effects of fluid flow, heat transfer, mass transfer and magnetic field are illustrated in Figs. 4–8 for different values of the parameters Pr, Ra, Ha, ϕ, N, Le and A in a trapezoidal enclosure with linearly heated and diffusive left wall, uniformly heated and diffusive lower wall, cold and of zero diffusion gradient right wall, adiabatic top wall having zero diffusion gradient. Due to different boundary conditions, fluid flow

Table 2. Grid independence test for $|\psi|_{\max}$, $|\pi|_{\max}$ and $|\tau|_{\max}$ for $A = 0.5$, $Pr = 0.71$, $Ra = 10^3$, $Ha = 20$, $Le = 2$ $N = 1$ and $\phi = 45\,°$.

Grid	$|\psi|_{\max}$	$|\pi|_{\max}$	$|\tau|_{\max}$
21×21	0.12987	0.25192	0.25179
41×41	0.13387	0.25386	0.25374
81×81	0.13329	0.25341	0.25372

represents asymmetric circulations with respect to a vertical line closed to the left wall in all the figures (Figs. 4–8). It is also observed that the stream line contours towards left hot and diffusive wall occurs with positive values, i.e., anticlockwise circulations present near the left wall, whereas stream lines with negative stream function values representing clockwise circulations occur near the right cold and nondiffusive walls. Since the upper wall of the cavity is moving with uniform velocity from left to right (lid driven upper wall), primary circulation cells of ψ-contours occupy a larger right portion of the cavity with respect to circulation in the left side of the cavity.

Figure 4 represents ψ, θ, S, π, τ, S_ψ, S_θ, S_τ, S_M and S_T contours for $Ra = 10^3$, $Ha = 20$, $N = 1$, $Pr = 0.7$, $Le = 2$, $\phi = 45\,°$ with $A = 0.5 - 1.5$, i.e., the effect of aspect ratio are depicted in this figure with $|\psi|_{\max} = 0.1333$ ($A = 0.5$); 0.3986 ($A = 1$); 0.6548 ($A = 1.5$), $|\pi|_{\max} = 0.2564$ ($A = 0.5$); 0.4799 ($A = 1$); 0.6892 ($A = 1.5$), $|\tau|_{\max} = 0.2577$ ($A = 0.5$); 0.4773 ($A = 1$); 0.6837 ($A = 1.5$), $|S_\psi|_{\max} = 1.2421$ ($A = 0.5$); 2.4262 ($A = 1$); 3.1629 ($A = 1.5$), $|S_\theta|_{\max} = 111111$ ($A = 0.5$); 27777 ($A = 1$); 12345 ($A = 1.5$), $|S_\tau|_{\max} = 56666$ ($A = 0.5$); 14166 ($A = 1$); 6296 ($A = 1.5$), $|S_M|_{\max} = 0.6286$ ($A = 0.5$); 1.0324 ($A = 1$); 3.9051 ($A = 1.5$) and $|S_T|_{\max} = 5.0023$ ($A = 0.5$); 4.8293 ($A = 1$); 5.6873 ($A = 1.5$). As aspect ratio increases, it is observed that entropy generation increases due to fluid friction and due to the effect of magnetic field, but decreases due to heat transfer and mass transfer. The effect of entropy generation due to heat and mass transfer are much higher than that due to fluid friction and magnetic field. Therefore, to increase the efficiency of any system, the aspect ratio of the enclosure should be higher as much as possible, which minimizes the total entropy generation. The contours of θ and S are smooth and converges to the right bottom corner, the junction of hot-massive and cold-nonmassive walls. So, the significant entropy generation due to heat and mass transfer is observed in the right bottom corner with higher values. The contours of S_ψ are dense along the top wall because of high velocity gradient due to adiabatic top wall, whereas the contours of S_M are dense in the right portion of the cavity with multiple circulation eddies for $A = 0.5, 1.0$, and for $A = 1.5$, they are distributed through out the cavity with small values of S_M at left bottom portion of the cavity. Contours of S_T are smoothly distributed for $A \leqslant 1$ and become complex for high aspect ratio forming a strong zone of entropy generation at right bottom corner.

Figure 5 represents ψ, θ, S, π, τ, S_ψ, S_θ, S_τ, S_M and S_T contours for $Ra = 10^3$, $Ha = 20$, $N = 1$, $Pr = 0.7$, $Le = 1$ and $A = 0.5$ for $\phi = 45\,°$, $60\,°$ and $90\,°$. It is observed that ψ contours make two kind of circulations with maximum values 0.1328, 0.1334 and 0.1233 for $\phi = 45\,°$, $60\,°$ and $90\,°$, respectively, and the maximum values occur near the center of the circulation cells. The contours of isotherms and isoconcen-
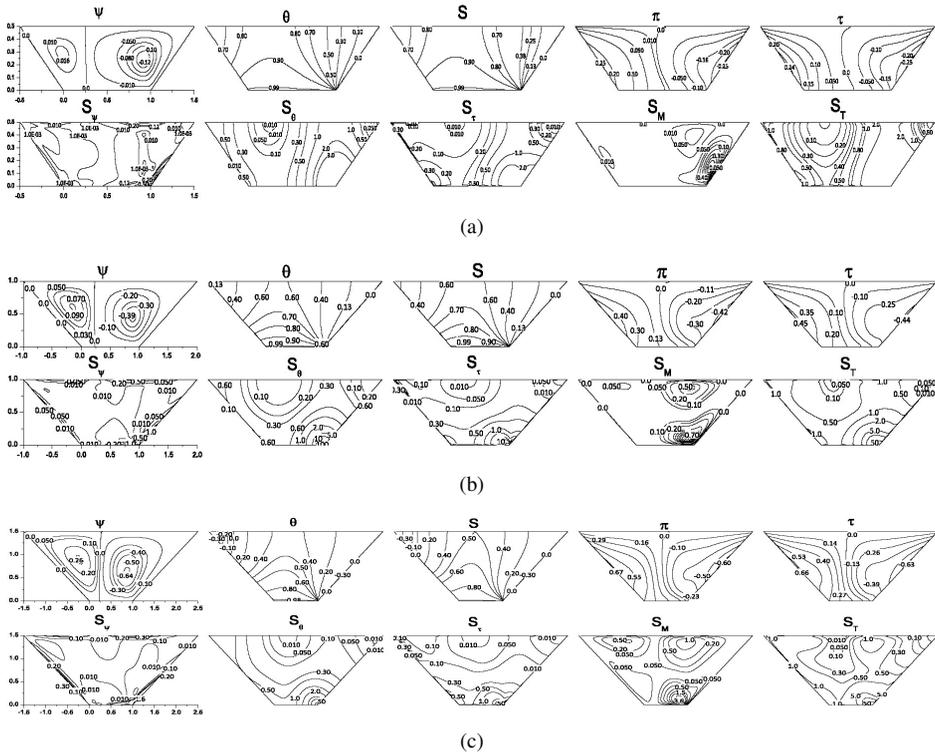
Figure 4. Stream lines (ψ), isotherms (θ), isoconcentrations (S), heat lines (π), mass lines (τ), entropy generations due to fluid friction (S_ψ), heat transfer (S_θ), mass transfer (S_τ) magnetic field (S_M) and total entropy generation (S_T) for $Ra = 10^3$, $Ha = 20$, $N = 1$, $Pr = 0.7$, $Le = 2$ and $\phi = 45\,^\circ$ for (a) $A = 0.5$, (b) $A = 1.0$ and (c) $A = 1.5$.

trations are smoothly distributed from left hot, massive wall to right bottom corner with $\theta \geqslant 0.9$ for $\phi = 45\,^\circ$ and $60\,^\circ$, but when $\phi = 90\,^\circ$ the same distribution is observed with $\theta \geqslant 0.8$. Thus more smooth and almost horizontal contours are observed when the inclination angle of the side walls of the cavity becomes $\phi = 90\,^\circ$. Heat line and mass line contours are distributed from bottom to left hot massive walls with positive values, i.e., in anticlockwise direction and to right cold, non massive walls with negative values, i.e., in clockwise direction with $|\pi|_{\max} = |\tau|_{\max} = 0.2564$ ($\phi = 45\,^\circ$); 0.2859 ($\phi = 60\,^\circ$); 0.3435 ($\phi = 90\,^\circ$). S_ψ contours are found to be compressed along the lower portion of the right wall and right portion of the left wall with $|S_\psi|_{\max} = 1.2438$ ($\phi = 45\,^\circ$); 1.1520 ($\phi = 60\,^\circ$); 0.9204 ($\phi = 90\,^\circ$). A huge effect of ϕ on S_M contours are observed with $|S_M|_{\max} = 0.6241$ ($\phi = 45\,^\circ$); 0.3233 ($\phi = 60\,^\circ$); 6.2528 ($\phi = 90\,^\circ$). The contours are compressed with eddies near the right side of the top and bottom walls when $\phi = 90\,^\circ$ whereas eddies are compressed near the right sidewall together with contours of small values on the other parts for $\phi = 45\,^\circ$ and $60\,^\circ$. Moreover total entropy generation S_T increases as ϕ increases with the values $S_T = 4.9984$ (for $\phi = 45\,^\circ$), $S_T = 5.6027$ (for $\phi = 60\,^\circ$) and $S_T = 7.1412$ (for $\phi = 90\,^\circ$).
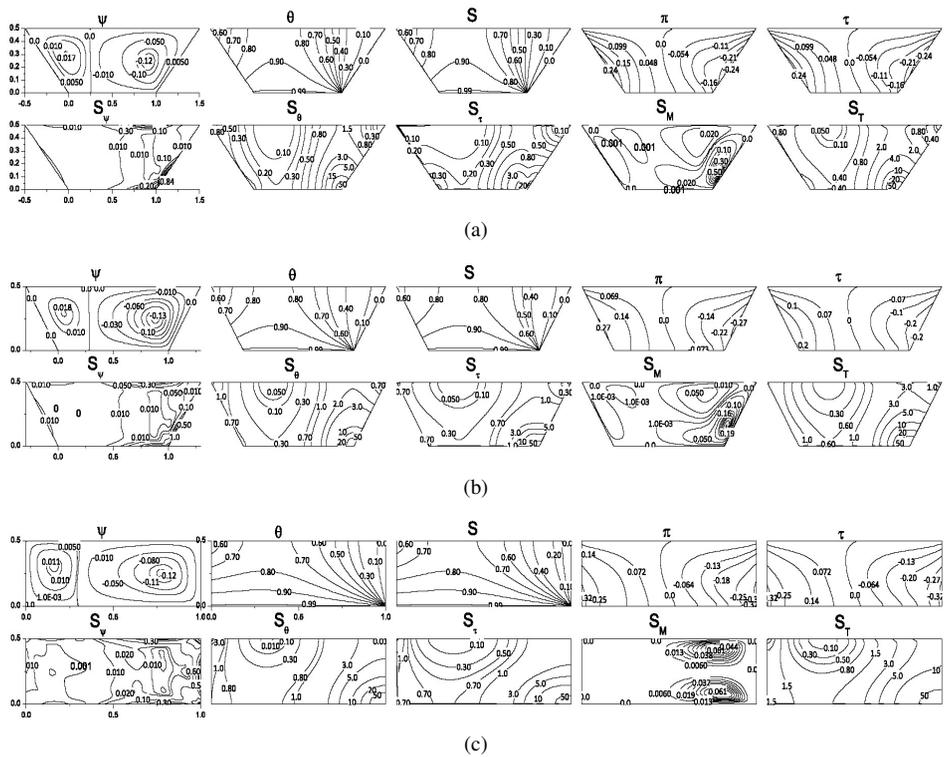
Figure 5. Stream lines (ψ), isotherms (θ), isoconcentrations (S), heat lines (π), mass lines (τ), entropy generations due to fluid friction (S_ψ), heat transfer (S_θ), mass transfer (S_τ) magnetic field (S_M) and total entropy generation (S_T) for $Ra = 10^3$, $Ha = 20$, $N = 1$, $Pr = 0.7$, $Le = 1$ and $A = 0.5$ for (a) $\phi = 45\,°$, (b) $\phi = 60\,°$ and (c) $\phi = 90\,°$.

When momentum diffusivity is much greater than thermal diffusivity, i.e., for large values of Pr, contours for ψ, θ, S, π, τ, S_ψ, S_θ, S_τ, S_M and S_T when $Ha = 20$, $N = 1$, $Le = 2$, $A = 0.5$, $\phi = 45°$ with different values of Ra (10^3, 10^4, 10^5) are shown in Figs. 6(a)–6(c). The values $\psi_{\min} = -0.1332\,(Ra = 10^3)$; $-1.2297\,(Ra = 10^4)$; $-5.1695\,(Ra = 10^5)$ indicate that when Pr is large, clockwise circulations rapidly increase towards the center of circulations with the increment of Ra. The contours of θ and S in Fig. 6 are almost similar to the previous observation in Fig. 5 for $Ra = 10^3$ and 10^4, but when $Ra = 10^5$, the contours become asymmetric due to high thermal and mass diffusivity. Heat line and mass line contours also change for large values of Ra (10^4, 10^5) and make two sided heat and mass circulation cells with $|\pi|_{\max} = 0.2564\,(Ra = 10^3)$; $0.7761\,(Ra = 10^4)$; $3.9372\,(Ra = 10^4)$, and $|\tau|_{\max} = 0.2577\,(Ra = 10^3)$; $0.8516\,(Ra = 10^4)$; $3.7714\,(Ra = 10^4)$ due to the effect of high convection. As Pr is the ratio of momentum diffusivity to thermal diffusivity, so large Pr implies momentum diffusivity is large compared to thermal diffusivity.

Nusselt number determines the quantity of heat exchanged between the fluid and the boundary, i.e., the ratio of convective to conductive heat transfer across the boundary.
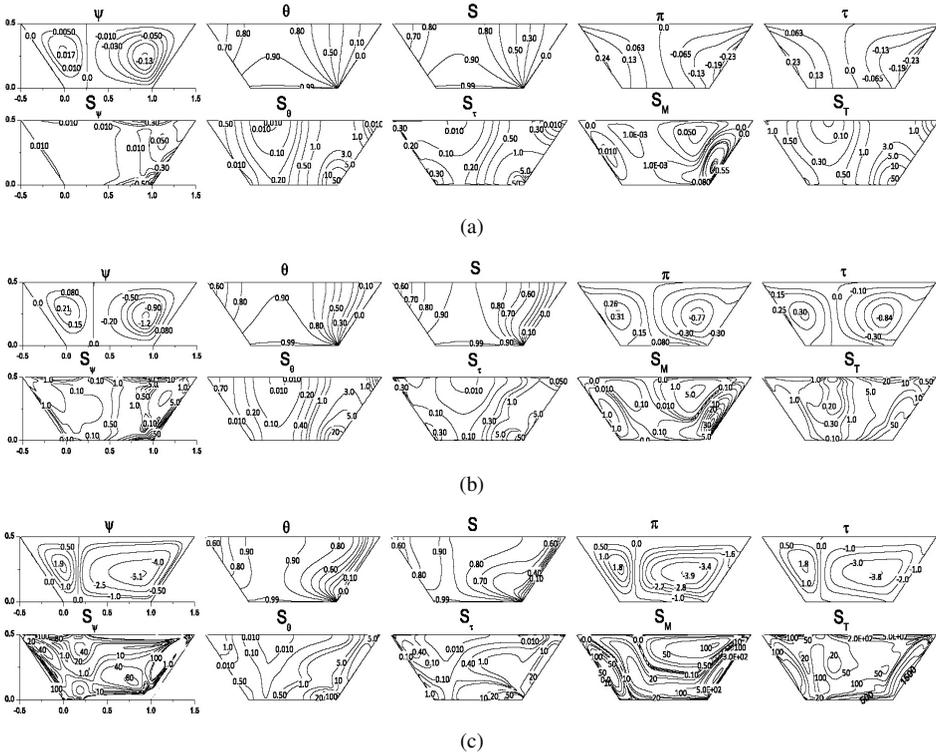
Figure 6. Stream lines (ψ), isotherms (θ), isoconcentrations (S), heat lines (π), mass lines (τ), entropy generations due to fluid friction (S_ψ), heat transfer (S_θ), mass transfer (S_τ) magnetic field (S_M) and total entropy generation (S_T) for $\phi = 45°$, $Ha = 20$, $N = 1$, $Pr = 1000$, $Le = 2$ and $A = 0.5$ for (a) $Ra = 10^3$, (b) $Ra = 10^4$ and (c) $Ra = 10^5$.

Figure 7 represents the variations of average local Nusselt number at the bottom wall ($\overline{Nu_b}$), average local Nusselt number at left wall ($\overline{Nu_l}$), average local Sherwood number at the bottom wall ($\overline{Nu_b}$) and average local Sherwood number at the left wall ($\overline{Nu_l}$) with Rayleigh number (Ra) for different values of ϕ at $Pr = 1000$, $Le = 2$, $N = 1$. As Nusselt number, a heat transfer coefficient represents the quality of heat transfer rather than the quantity at the boundary, it is observed that at the uniformly heated bottom wall of the cavity the qualitative heat transfer $\overline{Nu_b}$ is strictly increasing with respect to Ra and also increases as inclination angle ϕ increases. But along the linearly heated left wall, $\overline{Nu_l}$ is decreasing slowly for $\phi = 45°$ and $60°$ and decreasing in a quantitatively higher rate for $\phi = 90°$. It is also observed that $\overline{Nu_l}$ decreases with the increment of ϕ. The same observations as in the case of $\overline{Nu_b}$ follow for $\overline{Sh_b}$ but it is observed that $\overline{Sh_l}$ remains almost uniform for the increment of Ra when Ra is large with approximate values $\overline{Sh_l} = 0.2$ (for $\phi = 45°$), $\overline{Sh_l} = 0.32$ (for $\phi = 60°$) and $\overline{Sh_l} = 0.6$ (for $\phi = 90°$ and $Ra \geqslant 20000$). Therefore, it is clearly depicted in Fig. 7 that heat and mass transfer in the bottom wall of the cavity are much greater than that along left wall due to uniform heat and mass transfer at the bottom wall and linear heat and mass transfer at left wall.
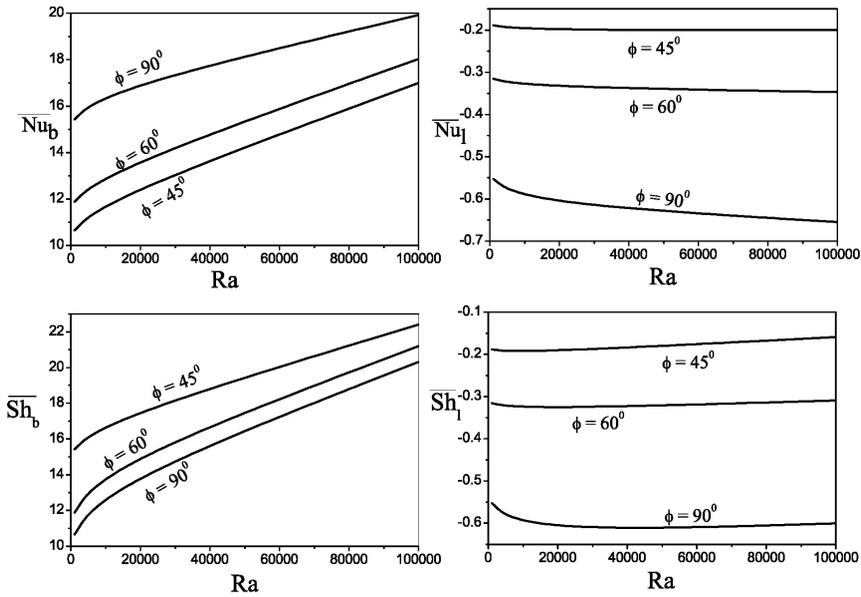
Figure 7. Variation of average local Nusselt number at the bottom wall ($\overline{Nu_b}$), average local Nusselt number at left wall ($\overline{Nu_l}$), average local Sherwood number at the bottom wall ($\overline{Nu_b}$) and average local Sherwood number at the left wall ($\overline{Nu_l}$) with Rayleigh number (Ra) for different values of ϕ at $Pr = 1000$, $Le = 2$, $N = 1$.
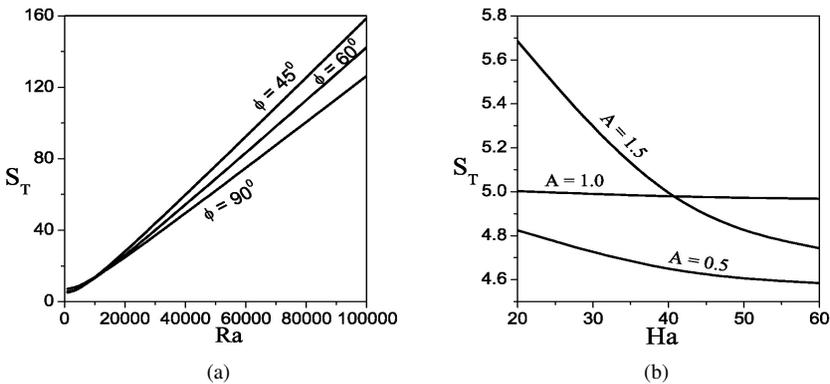
Figure 8. Variation of total entropy generation (S_T) with Ra and Ha for different values of ϕ and A, respectively, at $Pr = 1000$, $Le = 2$ and $N = 1$.

Total entropy generation throughout the cavity has huge importance for the efficiency of any system. In Fig. 8, the variation of total entropy generation is shown with respect to the change of Rayleigh number and Hartmann number for various values of inclination angle and aspect ratio of the cavity, respectively. From Fig. 8(a) it is observed that for a fixed value of ϕ, S_T is increasing very quickly with the increment of Ra and when the value of ϕ increases, S_T decreases.

In Fig. 8(b), the variation of S_T with Ha for various values of A are shown. It is clear from the figure that the total entropy generation is decreasing with the increment of Ha. It is also observed that as A increases, the total entropy generation decreases. Therefore, when the intensity of magnetic field is very high, cavities of high aspect ratios are preferable to minimize the total entropy generation.

8   Conclusions

In the present study, the analysis of stream lines, heat lines, mass lines and entropy generation due to fluid friction, heat transfer, mass transfer and magnetic field within a trapezoidal enclosure with various inclination angles and various aspect ratios with lid-driven upper wall has been carried out. From the present study the following conclusions can be drawn:

- When the aspect ratio is low, higher values of ϕ leads to an intensification of total entropy generation. Therefore, in case of air cooling system (specially for the cooling of electronic components) or any system with low Pr the enclosure of small ϕ together with small aspect ratio (A) can be used to reduce the loss of energy and to get maximum efficiency of the system.
- In the case of large Pr (e.g., ogive or engine oil with $Pr = 1000$), it is noticed that the absolute values of stream function, heat function, mass function, entropy due to fluid friction and magnetic field are highly increasing, whereas entropy generation due to thermal gradient and mass gradient are uniform with the increment of Rayleigh number and ultimately the total entropy generation is increasing.
- The effect of magnetic field is observed as follows. As the value of Ha is increasing total entropy generation is decreasing and the increased value of aspect ratio leads to decrease of an intensification of total entropy generation. Therefore, the cavity with high aspect ratio should be used when the intensity of the magnetic field is high.
- As Ra increases both heat transfer coefficient in terms of average Nusselt number at bottom wall ($\overline{Nu_b}$) and mass transfer coefficient in terms of average Sherwood number at the bottom wall ($\overline{Sh_b}$) increase for increased values of ϕ, which leads to high heat and mass transfer at the bottom wall but in the left wall $\overline{Nu_l}$ and $\overline{Sh_l}$ are almost uniform.

Appendix

$$E = \frac{2(1-2\xi)\cot\phi}{A(1+2A\eta\cot\phi)}, \qquad F = \frac{1+(1-2\xi)^2\cot^2\phi}{(1+2A\eta cot\phi)^2}, \qquad G = \frac{1}{(1+2A\eta\cot\phi)},$$

$$H = -\frac{4(1-2\xi)cot^2\phi}{(1+2A\eta\cot\phi)^2}, \qquad A_K = PrH - uG - \frac{vAE}{2},$$

$$T_1 = 3PrH - 4PrAEFG\cot\phi + A_KF,$$

$$T_2 = 2PrFH + 2PrEH - \frac{8}{A}PrFG\cot\phi + A_KE - \frac{vF}{A},$$

$$T_3 = \frac{3}{A^2}PrH - \frac{4}{A}PrEG\cot\phi + \frac{A_K}{A^2} - \frac{vF}{A},$$

$$T_4 = 48PrFG^2\cot^2\phi + 8PrEG^2\cot^2\phi + 8A^2PrE^2G^2\cot^2\phi$$
$$+ 2A_KH - \frac{v}{A}H,$$

$$T_5 = \frac{2}{A^2}PrF + PrE^2,$$

$$T_6 = 8PrA^2E^2G\cot^2\phi + 8PrEG^2\cot^2\phi + 24PrEG\cot^2\phi$$
$$+ A_KH - 2\frac{v}{A}H,$$

$$T_7 = -32PrEAG^3\cot^3\phi + 24PrHG^2\cot^2\phi + 8A_KG^2\cot^2\phi$$
$$- 8AEGv\cot^2\phi,$$

$$B_K = uG + \frac{AE}{2} - H, \qquad B_{Kc} = LeuG + \frac{AEv}{2}Le - H.$$

References

1. K. Al-Salem, H.F. Öztop, I. Pop, Y. Varol, Effects of moving lid direction on mhd mixed convection in a linearly heated cavity, *Int. J. Heat Mass Transfer*, **55**:1103–1112, 2012.

2. M. Alkasassbeh, Z. Omar, F.M. Oudina, J. Raza, A. Chamkha, Heat transfer study of convective fin with temperature-dependent internal heat generation by hybrid block method, *Heat Transfer Asian Res.*, **48**(4):1225–1244, 2019.

3. T. Basak, P. Kumar, R. Anandalakshmi, S. Roy, Analysis of entropy generation minimization during natural convection in trapezoidal enclosures of various angles with linearly heated side wall(s), *Ind. Eng. Chem. Res.*, **51**:4069–4089, 2012.

4. A. Bejan, A study of entropy generation in fundamental convective heat transfer, *J. Heat Transfer, Trans. ASME*, **101**(4):718–725, 1979.

5. A. Bejan, *Entropy Generation Minimization*, CRC Press,, Boca Raton, FL, 1982.

6. A. Bejan, *Entropy Generation Through Heat and Fluid Flow*, Wiley & Sons, New York, 1994.

7. A. Carotenuto, N. Massarotti, A. Mauro, A new methodology for numerical simulation of geothermal down hole heat exchangers, *Appl. Therm. Eng.*, **48**:225–236, 2012.

8. R.D.M. Carvalho, L. Goldstein Jr., L.F. Milanez, Heat transfer analysis of digital transmission equipment with horizontally arranged printed circuit boards, *Heat Transfer Eng.*, **9**(3):44–53, 1988.

9. C.K. Cha, Y. Jaluria, Recirculating mixed convection flow for energy extraction, *Int. J. Heat Mass Transfer*, **27**:1801–1810, 1984.

10. C.T. Chen, H.I. Chen,   Multi-objective optimization design of plate-fin heat sinks using a direction-based genetic algorithm, *J. Taiwan Inst. Chem. Eng.*, **44**:257–265, 2013.

11. G.D. Davis, Natural convection of air in a square cavity: A bench mark numerical solution, *Int. J. Numer. Methods Fluids*, **3**:249–264, 1983.

12. M.M. Gupta, J.C. Kalita,   A new paradigm for solving Navier–Stokes equations: Stream-function–velocity formulation, *J. Comput. Phys.*, **207**:52–68, 2005.

13. M. Hasanuzzaman, H.F. Öztop, M.M. Rahman, N.A. Rahim, R. Saidur, Y. Varol, Magneto-hydrodynamic natural convection in trapezoidal cavities, *Int. Commun. Heat Mass Transfer*, **39**:1384–1394, 2012.

14. K. Hooman, H. Gurgenci, Porous medium modeling of air-cooled condensers, *Transp. Porous Media*, **84**:257–273, 2010.

15. S.H. Hussain,   Analysis of heatlines and entropy generation during double-diffusive MHD natural convection within a tilted sinusoidal corrugated porous enclosure, *Eng. Sci. Technol.*, **19**:926–945, 2016.

16. F.J.K. Ideriah, Prediction of turbulent cavity flow driven by buoyancy and shear, *J. Mech. Eng. Sci.*, **22**:287–295, 1980.

17. G. Ilis, M. Mobedi, B. Sunden,   Effect of aspect ratio on entropy generation in a rectangular cavity with differentially heated vertical walls, *Int. Commun. Heat Mass Transfer*, **35**:696–703, 2008.

18. J. Imberger, P. F. Hamblin,   Dynamics of lakes, reservoirs and cooling ponds, *A. Rev. Fluid Mech.*, **14**:153–187, 1982.

19. S. Kimura, A. Bejan, The heatline visualization of convective heat transfer, *J. Heat Transfer*, **105**:916–919, 1983.

20. T.R. Mahapatra, B.C. Saha, D. Pal, Magnetohydrodynamic double-diffusive natural convection for nanofluid within a trapezoidal enclosure, *Comput. Appl. Math.*, **37**::6132–6151, 2018, `https://doi.org/10.1007s40314-018-0676-5`.

21. M. Mourad, A. Hassen, H. Nejib, B.B. Ammar,   Second law analysis in convective heat and mass transfer, *Entropy*, **8**(1):1–17, 2006.

22. F.M. Oudina, Numerical modeling of the hydrodynamic stability in vertical annulus with heat source of different lengths, *Eng. Sci. Technol.*, **20**:1324–1333, 2017.

23. F.M. Oudina, R. Bessaïh, Numerical modeling of MHD stability in a cylindrical configuration, *J. Franklin Inst.*, **351**:667–681, 2014.

24. F.M. Oudina, O.D. Makinde, Numerical simulation of oscillatory MHD natural convection in cylindrical annulus: Prandtl number effect, *Defect Diffus. Forum*, **387**:417–427, 2018.

25. L.A.B. Pilkington,   Review lecture: The float glass process, *Proc. R. Soc. Lond., Ser. A*, **IA314**:1–25, 1969.

26. D. Ramakrishna, T. Basak, S. Roy,   Analysis of heatlines and entropy generation during free convection within trapezoidal cavities, *Int. Commun. Heat Mass Transfer*, **45**:32–40, 2013.

27. J. Raza, F.M. Oudina, A.J. Chamkha,   Magnetohydrodynamic flow of molybdenum disulfide nanofluid in a channel with shape effects, *Multidiscipline Modeling in Materials and Structures*, **15**(4):737–757, 2019.

28. F. Selimefendigil, H.F. Öztop, Analysis of MHD mixed convection in a flexible walled and nanofluids filled lid-driven cavity with volumetric heat generation, *Int. J. Mech. Sci.*, **118**:113–124, 2016.

29. M.A. Sheremet, T. Grosan, I. Pop, Natural convection and entropy generation in a square cavity with variable temperature side walls filled with a nanofluid: Buongiornos mathematical model, *Entropy*, **19**(7):337, 2017, `https://doi.org/10.3390/e19070337`.

30. M.A. Sheremet, H.F. Öztop, I. Pop, N. Abu-Hamdeh, Analysis of entropy generation in natural convection of nanofluid inside a square cavity having hot solid block: Tiwari and Das' model, *Entropy*, **18**(1):9, 2016, `https://doi.org/10.3390/e18010009`.

31. M.A. Sheremet, I. Pop, H.F. Öztop, N. Abu-Hamdeh, Natural convection of nanofluid inside a wavy cavity with a non-uniform heating: Entropy generation analysis, *Int. J. Numer. Methods Heat Fluid Flow*, **27**:958–980, 2017.

32. A.K. Singh, T. Basak, A. Nag, S. Roy, Role of entropy eeneration on thermal management during natural convection in tilted porous square cavities, *J. Taiwan Inst. Chem. Eng.*, **50**:153–172, 2015.

33. N. Targui, H. Kahalerras, Analysis of fluid flow and heat transfer in a double pipe heat exchanger with porous structures, *Energy Convers. Manage.*, **49**:3217–3229, 2008.

34. M.A. Teamah, A.I. Shehata, Magnetohydrodynamic double diffusive natural convection in trapezoidal cavities, *Alexandria Eng. J.*, **55**:1037–1046, 2016.

35. D.V. Trevisan, A. Bejan, Combined heat and mass transfer by natural convection in a vertical enclosure, *J. Heat Transfer*, **109**:104–112, 1987.

36. H.M. Yeh, Upward type flat plate solar air heaters attached with fins and operated by an internal recycling for improved performance, *J. Taiwan Inst. Chem. Eng.*, **43**:235–240, 2012.